

# Stability of Solid Electrolyte Interphase Components on Lithium Metal and Reactive Anode Material Surfaces

Kevin Leung,<sup>1\*</sup> Fernando Soto,<sup>2</sup> Kie Hankins,<sup>2</sup>  
Perla B. Balbuena,<sup>2</sup> and Katharine L. Harrison<sup>1</sup>

<sup>1</sup>*Sandia National Laboratories, MS 1415,  
Albuquerque, NM 87185*

<sup>2</sup>*Department of Chemical Engineering,  
Texas A&M University,  
College Station, TX 77843*

\*kleung@sandia.gov

(Dated: May 24, 2016)

## Abstract

Lithium ion batteries (LIB) can feature reactive anodes that operate at low potentials, such as lithium metal or silicon, passivated by solid electrolyte interphase (SEI) films. SEI is known to evolve over time as cycling proceeds. In this modeling work, we focus on the stability of two main SEI components, lithium carbonate ( $\text{Li}_2\text{CO}_3$ ) and lithium ethylene dicarbonate (LEDC). Both components are electrochemically stable but thermodynamically unstable near the equilibrium  $\text{Li}^+/\text{Li}(\text{s})$  potential. Interfacial reactions represent one way to trigger the intrinsic thermodynamic instability. Both  $\text{Li}_2\text{CO}_3$  and LEDC are predicted to exhibit exothermic reactions on lithium metal surfaces, and the barriers are sufficiently low to permit reactions on battery operation time scales. LEDC also readily decomposes on high Li-content  $\text{Li}_x\text{Si}$  surfaces. Our studies suggest that the innermost SEI layer on lithium metal surfaces should be a thin layer of  $\text{Li}_2\text{O}$  – the only thermodynamically and kinetically stable component (in the absence of a fluoride source). This work should also be relevant to inadvertent lithium plating during battery cycling, and SEI evolution on  $\text{Li}_x\text{Si}$  surfaces.

## I. INTRODUCTION

Solid-electrolyte interphase (SEI) films that passivate low voltage anode surfaces are critical for lithium ion battery operations.<sup>1-6</sup> These films arise from electrochemical reduction and subsequent breakdown of the organic solvent-based electrolyte and additive molecules, which are unstable under battery charging potentials. The SEI blocks further electron transfer from the anode to the electrolyte, yet permits lithium ion ( $\text{Li}^+$ ) transport. SEI films on traditional graphite anodes are not static, but grow thicker during cycling. Moreover, they are known to evolve either by dissolution or chemical processes.<sup>7-10</sup> Silicon, a potential next-generation anode material,<sup>11</sup> can expand by 300% upon full lithiation, and the SEI films coating its surfaces<sup>12-20</sup> are likely to crack, delaminate,<sup>21,22</sup> and in general exhibit more dynamic evolution than on graphite surfaces. Lithium metal,<sup>23-25</sup> much more reactive than graphite, is also being considered as transportation battery anode material. Hence there is an urgent need for further understanding of SEI evolution and stability on these reactive anode surfaces.

In terms of SEI stability, SEI dissolution in liquid electrolytes has been discussed,<sup>26</sup> as has the chemical instability of SEI components due to elevated temperature,<sup>27,28</sup> the presence of acid,<sup>29</sup> and reactions with transition metal incorporated into the SEI.<sup>30,31</sup> A recent pioneering computational work that emphasizes the concept of SEI stability has predicted that organic SEI components can react with  $\text{Li}_x\text{Si}$  surfaces, as well as undergo attacks by radicals present in the electrolyte.<sup>32</sup> These interfacial reactions between SEI components and active materials help determine the chemistry at electrode/SEI interfaces. Understanding such reactions is crucial for generating detailed models of SEI structures that govern their electron-blocking and  $\text{Li}^+$  transmitting functions.

The present work systematically addresses the stability of multilayer organic and inorganic SEI components on Li metal and  $\text{Li}_x\text{Si}$  surfaces. This work is motivated by solid-solid interface modeling conducted in the context of lithium ion battery solid electrolytes,<sup>33-40</sup> and assumes a time lapse between the first deposition of SEI products and their destruction. Thus it is complementary to the liquid-solid interface approach<sup>32</sup> more pertinent to the initial stages of SEI growth.

First we distinguish three possible criteria of SEI stability: thermodynamic, electrochemical, and interfacial. (1) Following Ref. 41, we define “thermodynamic instability” to mean

that the bulk SEI material (assuming it can be synthesized in bulk quantity) can be decomposed into one or more solid or gas phases with lower overall free energy. This criterion allows breaking any chemical bond and is agnostic about reaction kinetics. (2) “Electrochemical instability” is taken to mean that the phase can be readily electrochemically oxidized or reduced during cyclic voltametry.<sup>42</sup> Only the cleavage of covalent or ionic bonds that can break in the time scale of electron transfer is permitted, although further work is needed to refine the precise meaning of the kinetic constraint. Electrochemical stability is related to band-alignment diagrams frequently invoked in the battery literature,<sup>41,43</sup> where redox reactions are assumed to begin when the Fermi levels in the metallic electrode coincide with the valence or conduction band edges of the electrolyte. However, organic electrolytes, SEI components such as  $\text{Li}_2\text{CO}_3$ , and many cathode oxide materials form localized charge states (“states in the gap”), or small polarons, upon being reduced or oxidized. Thus redox potentials, not band edge positions, are the rigorous governing quantities. Note that some authors describe this instability criterion as “thermodynamic”<sup>44</sup> rather than “electrochemical” (this work, Ref. 41, and others). (3) “Interfacial instability” here means that exothermic reactions can occur at the interface within typical lithium ion battery charge/discharge time scales. When a SEI component is thermodynamically unstable but electrochemically stable – thus preventing long-range electron transfer – interfacial reactions represent one key way to trigger the intrinsic thermodynamic instability. In this work, we impose a one-hour reaction time threshold; short reaction times are considered to yield interfacially instability.

This work focuses on two dominant SEI components, namely inorganic lithium carbonate ( $\text{Li}_2\text{CO}_3$ ) and organic lithium ethylene dicarbonate (LEDC). Both components are widely reported to be significant components of the anode SEI when the liquid electrolyte contains ethylene carbonate (EC) and other linear carbonates.<sup>2–4</sup> Crystalline Li(100) and amorphous silicon (a-Si) surfaces are used to represent two extremes of reactive anode surfaces on which the SEI may decompose. We stress that the a-Si/SEI interface is intended to represent SEI-covered Si anode surface after cycling, not pristine Si surfaces which should be covered with native oxides.<sup>45</sup> The SEI/Li(100) interface is relevant to undesirable Li-plating on graphite anodes<sup>47</sup> and intentional Li-deposition when Li metal is used as anode.<sup>48</sup> Li(100) may also be a reasonable proxy for high  $x$   $\text{Li}_x\text{Si}$  surfaces because in previous modeling studies,<sup>46</sup> the low energy surfaces of high- $x$   $\text{Li}_x\text{Si}$  are found to be dominated by Li atoms. Si outcroppings on Li(100) are considered for its effect on SEI reactivity in the supporting information document

(S.I.).

It has generally been accepted that anode SEI consists of an inner inorganic layer (e.g.,  $\text{Li}_2\text{CO}_3$ ,  $\text{Li}_2\text{O}$ , and/or  $\text{LiF}$ ) and an outer organic layer (e.g., LEDC and polymeric species).<sup>4,24</sup> However, the LEDC/ $\text{Li}(100)$  interface is relevant for reasons not just related to inadvertent Li-plating on the outer SEI surface.<sup>47</sup> A recent ultra-high vacuum (UHV) study has shown that LEDC can form from a sub-monolayer of EC molecules on Li metal surfaces at low temperature.<sup>49</sup> This finding is in agreement with a modeling work suggesting that LEDC may be formed by two-electron reduction of EC during the initial stages of SEI formation,<sup>50</sup> not (only) at late stages via one-electron reduction. Hence the reactions of LEDC on active material surfaces, presumably to produce inorganic species, are also relevant to the anode/SEI interface.

The voltage dependences of these processes will be discussed. By “voltage” we refer to the electronic potential,<sup>51</sup> which depends on the Fermi level and reflects the instantaneous applied potential. This definition is consistent with computational studies in many electrochemical applications.<sup>52–59</sup> In contrast, the lithium chemical potential, which is a function of the Li-content, is a slow-responding property that indicates whether the interfacial structure is out-of-equilibrium or not; at interfaces it does not by itself determine the instantaneous voltage.<sup>51</sup>

*Ab initio* molecular dynamics (AIMD) simulations are also conducted to show that decomposition reactions of organic SEI components similar to EDC can readily occur in less well-controlled, liquid-solid interface environments, with multiple species decorating the surfaces of  $\text{Li}_x\text{Si}$  crystalline anode with finite Li-content – instead of just  $\text{Li}(100)$  or Si-doped Li-metal surfaces. These simulations examine the decomposition of lithium vinylene dicarbonate ( $\text{Li}_2\text{VDC}$ ) during the initial stages of SEI formation, when liquid electrolyte,  $\text{LiF}$  clusters, and submonolayer  $\text{Li}_2\text{VDC}$  are all present. VDC differs from EDC only by a carbon-carbon double bond and two less protons. It can be formed in the presence of vinylene carbonate, a well-known electrolyte additive. The  $\text{LiF}$  cluster represents another surface “defect” on otherwise crystalline  $\text{Li}_x\text{Si}$ . The AIMD predictions in these systems complement and broadly agree with our static, solid-interface results. The reactions of  $\text{Li}_x\text{Si}$  with the other SEI component considered herein,  $\text{Li}_2\text{CO}_3$ , are more challenging due to the need for lattice matching between crystalline  $\text{Li}_2\text{CO}_3$  and the large  $\text{Li}_x\text{Si}$  surface unit cells.<sup>60,61,96</sup> Such studies will be conducted in the future.

This paper is organized as follows. Section II discusses the details of the DFT calculations. Section III describes the results. The implications of the predictions and comparison with experiments are discussed in Sec. IV, and Sec. V summarizes the paper.

## II. METHODS

We apply periodic boundary condition (PBC) DFT methods to assess thermodynamic stability and interfacial stability, and cluster-based (CB) DFT calculations to examine electrochemical stability. An SEI component is defined to be thermodynamically unstable if energy is gained by transforming it into other phases upon reaction with Li metal; to exhibit interfacial instability on a particular anode material surface if it reacts exothermically within one hour; and to exhibit electrochemical instability if CB-DFT predicts a reduction potential which is positive relative to the  $\text{Li}^+/\text{Li(s)}$  reference. If an SEI component reacts on an anode surface and transforms into a new stable phase or film which passivates the anode, the original SEI component is still regarded as unstable at the interface.

PBC DFT calculations are conducted using the Vienna Atomic Simulation Package (VASP) version 5.3.<sup>62-64</sup> Most calculations apply the PBE functional.<sup>65</sup> HSE06,<sup>66</sup> which exhibits less delocalization error,<sup>67</sup> is used to re-examine systems with marginal kinetic stability. A 400 eV planewave energy cutoff is applied in all cases. Since previous AIMD simulations of the initial stages of SEI formation have rarely yielded  $\text{CO}_3^{2-}$  and have predicted no LEDC,<sup>46,68</sup> configurations from AIMD trajectories are not used as input. Instead, we have constructed multi-layer  $\text{Li}_2\text{CO}_3$  (001) and LEDC slabs on anode material surfaces. Several simulation cells are depicted in Fig. 1, with further details listed in Table I. The climbing-image nudged elastic band method (NEB) is applied to predict reaction barriers.<sup>69</sup> A predicted reaction time scale of 1-hour requires that the total net reaction exhibits a negative free energy change and sufficiently low reaction barrier(s). If a typical vibrational frequency-related prefactor of  $k_o=10^{12}/\text{s}$  is assumed, the overall rate  $k = k_o \exp(-\Delta G^*/k_B T)$  is faster than 1/hour when all reaction barriers ( $\Delta G^*$ ) are at most 0.92 eV.

The standard dipole correction is applied to negate image interactions in the periodically replicated, charge-neutral simulation cells.<sup>70</sup> For a simulation cell with a metallic Li(100) slab and a vacuum region,  $E_F$  is well defined; the work function ( $\Phi$ ) is the difference between  $E_F$  and the vacuum level, and the electronic voltage is simply  $(\Phi/|e|-1.37)$  V vs.  $\text{Li}^+/\text{Li(s)}$ ,

system	dimensions	stoichiometry	$k$ -point	figure
EDC/Li(100)	$19.50 \times 19.50 \times 34$	$\text{Li}_{228}\text{C}_{72}\text{O}_{108}\text{H}_{72}$	$2 \times 2 \times 1$	1d,3,6,7
1-CO <sub>2</sub> /Li(100)	$30 \times 9.75 \times 9.75$	$\text{Li}_{48}\text{C}_1\text{O}_2$	$1 \times 2 \times 2$	5
EDC/a-Si	$16.75 \times 15.09 \times 38$	$\text{Si}_{127}\text{Li}_{38}\text{C}_{72}\text{O}_{108}\text{H}_{72}$	$1 \times 1 \times 1$	7
Li <sub>2</sub> CO <sub>3</sub> (001)/Li(100)	$25.02 \times 15.03 \times 34$	$\text{Li}_{324}\text{C}_{72}\text{O}_{216}$	$1 \times 2 \times 1^*$	1e,8a
1-Li <sub>2</sub> CO <sub>3</sub> /Li(100)	$30 \times 9.75 \times 9.75$	$\text{Li}_{52}\text{C}_1\text{O}_3$	$1 \times 2 \times 2$	8e,8f
Li <sub>2</sub> CO <sub>3</sub> (001)/a-Si	$16.68 \times 15.03 \times 34$	$\text{Si}_{127}\text{Li}_{96}\text{C}_{48}\text{O}_{144}$	$2 \times 2 \times 1$	1g,8a
Li <sub>2</sub> VDC/Li <sub>3.25</sub> Si(010)	$17.80 \times 15.94 \times 34$	$\text{Li}_{127}\text{Si}_{32}\text{F}_{48}\text{C}_{89}\text{O}_{99}\text{H}_{79}$	$2 \times 2 \times 1$	1h,9
Li <sub>2</sub> VDC/Li <sub>3.25</sub> Si(010)	$17.80 \times 15.94 \times 34$	$\text{Li}_{127}\text{Si}_{32}\text{C}_{20}\text{O}_{30}\text{H}_{10}$	$2 \times 2 \times 1$	10

TABLE I: Simulation cell size ( $\text{\AA}^3$ ), stoichiometry, and Brillouin zone sampling of some periodic boundary condition model systems considered in this work. “1-X” means only one formula unit of “X” is present. \*Increasing the  $k$ -point sampling to  $2 \times 3 \times 1^*$  changes the  $\text{CO}_3^{2-}$  decomposition barrier by less than 0.03 eV.

where  $|e|$  is the electronic charge. The “1.37” V value reflects the potential difference between an electron at infinity and inside a Li metal foil held at 0 V; it is independent of the SEI component. This electronic voltage is to be directly compared to the ideal applied experimental potential, i.e., it is assumed no ohmic loss exists.

Amorphous Si (a-Si) slabs are created by melting LiSi crystals at high temperature, quenching, cutting a surface, and gradually removing Li. a-Si slabs are insulating. The relevant  $E_F$  in this case should depend on impurity states inside the band gap. Since this work does not focus on defects, the voltage of a-Si cannot be unambiguously defined. Future modeling effort can address a-Si electronic voltages by doping with P and B atoms to create metallic a-Si models.<sup>71</sup> The effect of varying the charging rate can be qualitatively examined by setting unequal ionic and electronic voltages, thus imposing an overpotential on the system.

The VASP code is also used to conduct AIMD simulations with Li<sub>2</sub>VDC on anode surfaces. These simulations are conducted at T=450 K, using the NVT ensemble and a 1 fs time step.<sup>68</sup> The simulation cell contains a (010) Li<sub>13</sub>Si<sub>4</sub> slab and has dimensions  $17.80 \times 15.94 \times 25.00 \text{ \AA}^3$ . Note that the initial packing of the FEC molecules onto the anode surface containing an overlayer of LiVDC is created using the BIOVIA Materials Studio

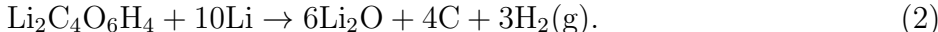
Amorphous Cell module.<sup>72</sup> The LiF unit cell from the crystallography open database<sup>73</sup> and the crystal builder option of the Materials Studio software are used to build a LiF model cluster on top of the anode surface (Fig. 1e-f). A LiF cluster with a 5 Å radius, consisting of a total of 18 Li and 18 F atoms, is selected for this study. The size was chosen to represent a seed of the nucleating LiF phase; other cluster sizes will be considered in the future. A 1.0 M LiPF<sub>6</sub> salt immersed in a pure FEC solvent (28 FEC molecules and two LiPF<sub>6</sub>) is used as the electrolyte solution that fills the gap between the two Li<sub>13</sub>Si<sub>4</sub> surfaces. As a first step, we employ the classical universal force field (UFF)<sup>74</sup> and the Forcite module in BIOVIA to pre-equilibrate the electrolyte portion of the system. The electronic voltage is not calibrated but is expected to be low.

Cluster-based calculations are conducted using the Gaussian (G09) suite of programs,<sup>75</sup> the DFT/PBE0 function,<sup>76</sup> and the “SMD” dielectric continuum approximation.<sup>77</sup> Liquid electrolytes with varying amounts of EC and dimethyl carbonate (DMC) or diethyl carbonate (DEC) used in batteries exhibit slightly different  $\epsilon_o$ . In this work, we have followed Ref. 50 and used a single  $\epsilon_o=40$  value. Geometry optimization is performed using a 6-31+G(d,p) basis set. Single point energies are computed at a 6-311++G(3df,2pd) level of theory. Vibrational frequencies are computed using the smaller basis, yielding zero point energies and thermal corrections.

### III. RESULTS

#### A. Thermodynamic Instability

First we consider the following solid or solid/gas phase reactions at zero temperature:



Here Li<sub>2</sub>C<sub>4</sub>O<sub>6</sub>H<sub>4</sub> is the chemical formula for a LEDC unit. All species are solids except those labeled as gas (“(g)”). Diamond is used to represent solid carbon. Its cohesive energy is similar to the slightly more stable graphite. The DFT method used herein is not dispersion-corrected and can underestimate graphite stability. We stress that it is unnecessary to find the most stable products; the existence of one set of product phases lower in free energy than

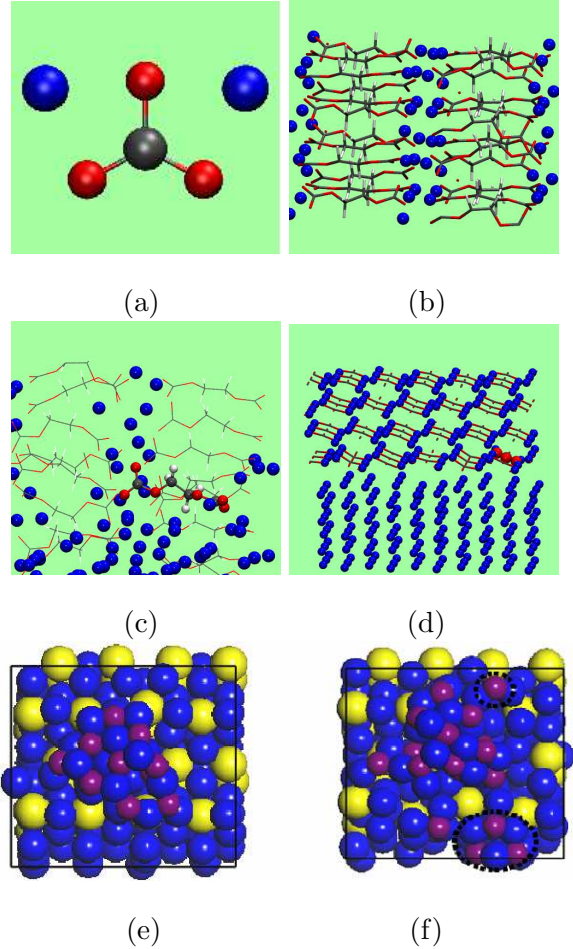


FIG. 1: (a)  $\text{Li}_2\text{CO}_3$  formula unit. (b)  $\text{Li}_2\text{C}_4\text{H}_4\text{O}_6$  (LEDC) “crystal,” optimized using DFT/PBE calculations. (c) 3-bilayer LEDC on Li(100). The strong interaction renders the initially crystalline Li surface almost amorphous. (d) 4-layer  $\text{Li}_2\text{CO}_3(001)$  on Li(100). Blue, grey, red, and white represent Li, C, O, and H atoms, respectively. Li, and molecular species which react with the anode surface, are depicted as ball-and-stick figures; non-reacting species are usually sticks or lines. (e) Top view of LiF cluster adsorbed on  $\text{Li}_{13}\text{Si}_4(010)$  surface. (f) The smaller sets of LiF pairs are shown inside the black circles. They result from  $\text{PF}_6^-$  decomposition or FEC reduction after 9.6 ps AIMD simulations (Sec. III F). Yellow spheres depict Si atoms in panels (g)&(h).

the original renders the latter thermodynamically unstable. The solid  $\text{Li}_2\text{CO}_3$  structure is well known,<sup>78</sup> as is body-centered-cubic Li. There are 2.6 % and 2.8 % lattice mismatches between the  $5\times 3$  Li(001) and  $3\times 3$   $\text{Li}_2\text{CO}_3(001)$  slabs in the lateral directions (Table I), and lithium metal is stretched by these amounts. No crystal structure is available for LEDC, and lattice matching information cannot be inferred. However, molecular dynamics simulations



have revealed a layered structure.<sup>79</sup> Our 3-bilayer LEDC simulation cell (Fig. 1c) is obtained by optimizing two staggered layers of LEDC molecules.

From DFT/PBE calculations, Eqs. 1 and 2 are exothermic by 1.29 eV and 1.22 eV per Li consumed. The fundamental reason for  $\text{Li}_2\text{CO}_3$  instability is the fact that carbon atoms with formal charge states of (+4) are in the presence of the extremely electronegative lithium metal. Finite temperature effects, ignored herein, may make Eq. 2 even more favorable due to gas phase entropy production. Replacing “C” with  $\text{Li}_2\text{C}_2$  also changes the energetics.<sup>80</sup> Extrapolating from these predictions, it is likely that many carbon-containing SEI components with high formal charges on carbon are thermodynamically unstable in the presence of low-potential, lithium-containing anodes.

In the formulation of Ref. 41, Eqs. 1 and 2 should correspond to equilibrium reduction potentials of 1.29 and 1.22 V vs.  $\text{Li}^+/\text{Li}(\text{s})$  for  $\text{Li}_2\text{CO}_3$  and LEDC. However, the breaking of many ionic or covalent bonds are needed to achieve the phase transitions, which may consequently be kinetically hindered. To our knowledge, no reduction signature for  $\text{Li}_2\text{CO}_3$  and LEDC at  $> 1$  V has been reported in cyclic voltametry. We note that CV curves can be difficult to analyze, as they convolve contributions from electrochemical reactions of fluoride-containing binders and metal oxides. However,  $\text{Li}_2\text{CO}_3$  obtained from  $\text{CoCO}_3$  can be electrochemically reduced to  $\text{Li}_2\text{O}$  and carbide via conversion reactions.<sup>80</sup>

## B. Electrochemical Stability

Another definition of instability for  $\text{Li}_2\text{CO}_3$  and LEDC is related to their reduction potential ( $\Phi$ ).  $-|e|\Phi$  gives the (free) energy gained when injecting an electron from an electrode held at 0 V vs.  $\text{Li}^+/\text{Li}(\text{s})$ .

To estimate the reduction thresholds, we take a single formula unit of  $\text{Li}_2\text{CO}_3$  (Fig. 1a) and LEDC (Fig. 1b), embed each into the SMD dielectric continuum,<sup>77</sup> and perform cluster-based DFT/PBE0 calculations to evaluate the free energy difference between LEDC and  $\text{LEDC}^-$ , and between  $\text{Li}_2\text{CO}_3$  and  $\text{Li}_2\text{CO}_3^-$ . These calculations assume a high, liquid-electrolyte-like dielectric constant ( $\epsilon_o$ ), are pertinent to SEI products in liquid or at liquid-SEI interfaces, and likely overestimate  $\Phi$  and the stability of SEI products inside the lower dielectric regions of solid SEI phases, for which crystal structures are frequently lacking.

By manually deforming one of the two  $\text{CO}_3$  groups in LEDC into a tetrahedral,  $sp^3$ -

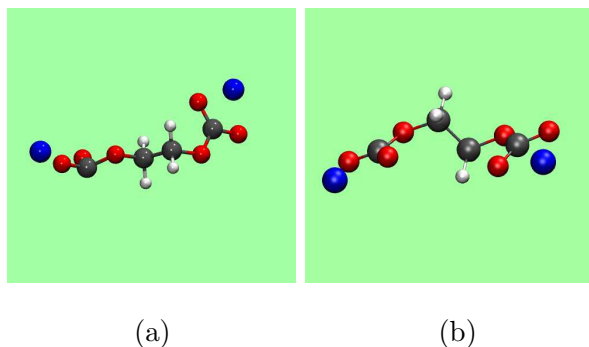


FIG. 2: (a) LEDC unit with excess electron on left-most carbonyl carbon, bent out of the plane formed by its three oxygen neighbors; (b) LEDC without an excess electron.

like geometry, we manage to deposit an excess  $e^-$  on that deformed  $\text{CO}_3$  group (Fig. 2a). The optimized configuration is substantially distorted from the initial optimized, unreduced LEDC geometry (Fig. 2b). It has O-C-O angles of  $109.7^\circ$ ,  $114.4^\circ$ , and  $116.6^\circ$ , and more significantly, the C-atom is out of the plane formed by the three O atoms by  $0.35 \text{ \AA}$  instead of being co-planar in the uncharged case. The predicted  $\Phi$  is  $-0.44 \text{ V vs. Li}^+/\text{Li(s)}$ , which is outside the operating window of lithium ion batteries. Attempts to inject an  $e^-$  into the  $\text{CO}_3^{2-}$  unit<sup>82</sup> invariably leads to one of the  $\text{Li}^+$  ion being reduced to a charge-neutral Li radical instead, along with a negative  $\Phi = -0.40 \text{ V vs. Li}^+/\text{Li(s)}$ .<sup>83,84</sup> We conclude that both LEDC and  $\text{Li}_2\text{CO}_3$  are electrochemically stable under normal battery operating conditions. For either to accept  $e^-$  from the anode, reactions triggered by the interface or other chemical means are required.

### C. Interfacial Instability: LEDC on Li(100)

In the remainder of this section, we focus on interfacial studies. Figure 1d depicts a 3-bilayer LEDC slab on the Li(100) surface. We use the climbing-image NEB technique to examine the reaction energetics of a EDC with one  $-\text{CH}_2\text{O}(\text{C}=\text{O})\text{O}^-$  group close to and parallel to the Li metal surface. The reaction end product, with a broken C-O bond and a released  $\text{CO}_2^{2-}$  which binds to the Li surface (Fig. 3a),<sup>85,86</sup> is exothermic by  $1.94 \text{ eV}$  (Fig. 4a). The DFT/PBE-predicted reaction barrier of  $\Delta E^* = 0.22 \text{ eV}$  associated with the transition state (Fig. 3b) is low enough to permit sub-hourly reactions. While the PBE functional can slightly underestimate reaction barriers, this small  $\Delta E^*$  means that using a more accurate

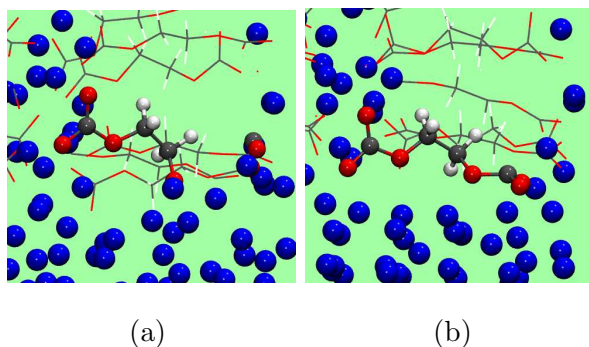


FIG. 3: (a) LECD on Li(100) with broken C-O bond and  $\text{CO}_2$  unit on Li surface; (b) reaction transition state. See Fig. 1c, which depicts the unreacted interface, for color key.

DFT functional is unlikely to change our qualitative conclusion about the reaction time scale.

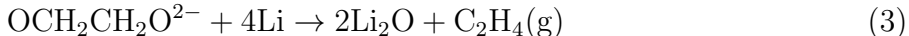
The electronic voltages of this interface with/without LECD decomposition, computed using the work function approach,<sup>51</sup> are  $-0.08$  V and  $-0.06$  V vs.  $\text{Li}^+/\text{Li(s)}$  before and after C-O bond cleavage. They are only slightly below the Li-intercalation voltage for Si. Only small changes in the potential accompany in this charge-transfer reaction, unlike in Ref. 57. This is partly because the voltage change after charge transfer is inversely proportional to the simulation cell surface area, which is much larger in our system (Table I). Our attempt to increase the voltage by removing  $\text{Li}^+$  at interfaces and creating favorable dipole moments<sup>51</sup> leads to diffusion of  $\text{Li}^+$  from the outer region to the inner region that negates the intended, initially observed voltage increase. Thus we have omitted voltage control for LECD films (see however  $\text{Li}_2\text{CO}_3$  below).

Soto *et al.* have also reported EDC decomposition in unconstrained, picosecond-long AIMD simulations, including  $\text{CO}_2^{2-}$  and  $\text{CO}_3^{2-}$  detachment from LECD, in the absence or presence of radicals in the solution.<sup>32</sup> That work was performed on 2 layers of LECD on Li-rich  $\text{Li}_x\text{Si}$  surfaces. This suggests that interfacial chemical reactions are not affected by the thickness of the LECD film or the precise chemical/dielectric medium in which the EDC unit resides. A recent UHV measurement has shown that LECD can be stabilized on lithium metal surfaces at  $T=100$  K.<sup>49</sup> The voltage under UHV conditions should be close to the bare Li(100) value of 1.56 V.<sup>51</sup> In light of the present work, SEI decomposition on lithium surfaces at  $T>100$  °C temperature in UHV conditions, with an applied electric field to mimic low-voltage conditions, may be of significant interest. Finally, reactions involving

oligomerization<sup>32,87</sup> or proton transfer<sup>88</sup> may occur, but the  $\text{CO}_2^{2-}$  release route is already sufficiently fast to ensure that decomposition takes place. For the same reason, we have not examined the effect of LEDC orientation on its decomposition pathways on Li(100).

The  $\text{CO}_2^{2-}$  fragment on Li(100) surfaces can further react. The barrier associated with breaking one of its C-O bonds ( $\Delta E^*=0.78$  eV) is somewhat higher than the first EDC decomposition step. The reaction is also less exothermic ( $\Delta E=-0.97$  eV, Fig. 4b), but should readily proceed within battery operation time scales. It is unnecessary to compute the barrier associated with CO reactions on Li(100); in a previous AIMD simulation, CO breakdown into C and O dispersed inside Li metal has been observed within picoseconds.<sup>81</sup> The role of  $\text{CO}_2$  in improving the anode SEI has been discussed in the literature.<sup>89,90</sup>

Finally, we examine the interfacial stability of the alkoxide terminus ( $-\text{CH}_2\text{O}^-$ ) coordinated to Li metal surface, left over from the release of  $\text{CO}_2$  from EDC. While the reaction is exothermic, the barrier is almost 1.8 eV (Fig. 4a). From this calculation, we infer that



will not proceed on Li metal surfaces on timescales relevant to battery operations. X-ray photoelectron spectroscopy measurements have reported the existence of alkoxide groups near lithium metal surfaces,<sup>23,24</sup> and Li-C bonds have also been reported.<sup>23</sup> Our calculations suggest the latter may arise from breakdown of  $\text{CO}_2^{2-}$  fragments. Some alkoxide groups may further react with organic carbonate molecules.<sup>50,91</sup>

In summary, LEDC is predicted to decompose into  $\text{O}^{2-}$ , carbon (either as lithium carbide or graphite), and  $\text{OC}_2\text{H}_4\text{O}^{2-}$  on Li(100) surfaces.

#### D. Interfacial Stability: LEDC on a-Si

Figure 5a depicts a 3-bilayer LEDC film on a-Si surface. The interface model originates from LEDC adsorbed on LiSi. Li atoms are sequentially removed from LiSi and the lateral dimensions of the simulation cell are contracted in stages. Due to the contraction, EDC appear buckled with their ionic termini bent towards the surface. Motivated by the predictions on Li-rich surfaces, we attempt to break a C-O bond on a EDC molecule to release a  $\text{CO}_2$  group which becomes bonded to a surface Si atom via its C-site (Fig. 5b). (This LEDC molecule chosen to react has one carbonyl C atom closest to an Si atom, and should react

most readily among those adsorbed on the surface.) The reaction is slightly exothermic at zero temperature ( $\Delta E = -0.17$  eV), and the overall barrier is  $\Delta E^* = 0.95$  eV (Fig. 4d), slightly higher than the  $< 0.92$  eV kinetic criterion discussed in the Method section. This shows that LEDC is kinetically barely stable on discharged silicon anode surfaces. It cannot be ruled out that other starting configurations on the amorphous Si surface may yield slightly lower reaction barriers, but LEDC reactivity is clearly much lower on a-Si than Li(100).

### E. Interfacial Instability: $\text{Li}_2\text{CO}_3$ on Li(100)

$\text{Li}_2\text{CO}_3$  is thermodynamically unstable at voltages near Li-plating when excess Li is available (Eq. 1). The only question is whether a kinetically viable pathway allows this and related reactions. Figure 6 depicts  $\text{Li}_2\text{CO}_3$  decomposition on Li(100). Initially we place a 4-layer  $\text{Li}_2\text{CO}_3$  (001) slab on Li(100) and optimize the geometry (Fig. 1e). Substantial deformation of the soft lithium metal surface accommodates the presence of the carbonate film.<sup>92</sup> Breaking a C-O bond at the interface, leaving a  $\text{CO}_2^{2-}$  anion in the carbonate layer while depositing an oxygen anion on the Li surface (Fig. 6a), is exothermic by  $-0.82$  eV. The overall transition state barrier energy (Fig. 4d) is 1.19 eV, meaning that this reaction is too slow to occur during battery operations.

However,  $\text{CO}_3^{2-}$  decomposition can be facilitated by excess Li. When two Li atoms are added in what appears to be an empty crevice between Li(100) and  $\text{Li}_2\text{CO}_3$ (001) (Fig. 6b), the total energy of the simulation cell is only 0.14 eV higher after subtracting the chemical potentials ( $\mu_{\text{Li}}$ ) of the two added Li, which are assumed to be the  $\mu_{\text{Li}}$  of Li metal. At higher equilibrium potentials, the cost will be larger, which slightly increases the overall barrier. Configurations with excess Li at the interface may be inevitably present during charging, because Li has to pass through the interface.

Figures 6b-6d revisit  $\text{CO}_3^{2-}$  decomposition when these two Li are present. In contrast to the case without additional Li atoms, a metastable reaction intermediate can be stabilized. It consists of the decomposing  $\text{CO}_3^{2-}$  adopting a bent geometry, with excess  $e^-$  on the C atom (Fig. 6c). The rate-determining barrier to reach this intermediate is  $\Delta E^* = 0.66$  eV (Fig. 4e), much reduced from the case without the two additional interfacial Li (Fig. 4d). The further reaction to break a C-O bond in the bent  $\text{CO}_3^{2-}$  and release  $\text{O}^{2-}$  is exothermic, with the energy released exceeding the cost of initially adding the two Li. This second reaction step

exhibits a minimal barrier (Fig. 4e).<sup>94</sup> The two added Li apparently make the reaction zone more  $e^-$  rich and stabilize the  $\text{CO}_2^{2-}$  product. In fact, by placing 18 extra Li atoms into interfacial crevices (not shown), we have observed several spontaneous, barrierless  $\text{CO}_3^{2-} \rightarrow \text{CO}_2^{2-} + \text{O}^{2-}$  reactions there. However, the resulting total energy is less favorable than without those Li extra atoms when  $\mu_{\text{Li}}$  is accounted for, likely because some of the added Li are undercoordinated.

The time scale associated with  $\text{planar-CO}_3^{2-} \rightarrow \text{bent-CO}_3^{4-}$ , deformation (0.66 eV barrier) is estimated to be 0.12 s, within battery operation timescale but far beyond AIMD trajectory lengths. This emphasizes the need to calculate barriers, using either static NEB calculations or liquid state potential-of-mean-force techniques as appropriate.

We also consider a single  $\text{CO}_3^{2-}$  adsorbed on Li(100) (Fig. 6e). This system involves a much smaller simulation cell and permits the use of more accurate DFT functionals to re-examine the rate-determining barrier required to reach the deformed  $\text{CO}_3$  intermediate. Four Li atoms decorate the area around the anion so that a bent, metastable  $\text{CO}_3$  (Fig 6f) can be stabilized at +0.76 eV vs. the original flat  $\text{CO}_3^{2-}$  geometry. The barrier leading to this intermediate is 0.76 eV. Using the generally more accurate DFT/HSE06 method instead of PBE used throughout this subsection, the barrier is increase only slightly to 0.86 eV. This demonstrates that there is no significant  $\Delta E^*$  dependence on DFT functionals. One reason is that this reaction intermediate involves molecular deformation rather than bond-breaking, and the DFT/PBE delocalization error should be less significant.<sup>67</sup> The deformation energy and electron reduction contributions to the energetics cannot be decoupled because electrons spontaneously flow to the deformed carbonate.

The electronic voltages of Figs. 6b-d are all 0.88 V vs.  $\text{Li}^+/\text{Li}(\text{s})$ . It can be argued that the inclusion of liquid electrolytes will reduce this value to approximately 0 V vs.  $\text{Li}^+/\text{Li}(\text{s})$  (in chemical equilibrium with the Li metal slab) due to preferential interfacial dipole moment alignment of organic solvent molecules.<sup>51,93</sup> Since liquid electrolyte is not considered in this section, we explore the effect of voltage variations by adding two Li interstitials between the outermost layers of  $\text{Li}_2\text{CO}_3$  (Fig. 6g). Bader analysis<sup>95</sup> shows that these Li spontaneously exhibit  $\text{Li}^+$  charge states, and their positive charges should be compensated by a negative surface charge density on Li(100) in the charge-neutral simulation cell. A large dipole moment is created, lowering the voltage from 0.88 V to  $-0.02$  V. Even though the overall potential is now significantly lower than that of Figs. 6b-d, and this should favors reductive

decomposition, the energies associated with  $\text{CO}_3^{2-}$  decomposition are almost unchanged. The bent  $\text{CO}_3$  intermediate and the broken C-O configurations are rendered more favorable only by 0.04 and 0.04 eV, respectively, compared to when the voltage is 0.88 V (Fig. 6b-d). The reason is that the electric field generated by the two  $\text{Li}^+$  interstitials is weak ( $\sim 0.9$  V/10 Å). This calculation suggests that, if the outer surface is occupied by a high-dielectric liquid with counter-ions, so that it is the electrolyte rather than interstitial  $\text{Li}^+$  that lowers the electronic voltage from 0.88 V to about 0 V, the effect on  $\text{Li}_2\text{CO}_3$  degradation at the solid-solid interface will still be small – just because of the thickness of the carbonate layer dictates a weak electric field.

The above system with a weak interfacial electric field assumes that the electric double layer (EDL) is not localized at the solid-solid interface (c.f. Fig. 1d or Fig. 1f in Ref. 51). Another possibility is that  $\text{Li}^+$  interstitials or vacancies right at the interface lead to a narrow EDL and a much larger local electric field just outside the active electrode material (Fig. 1e in Ref. 51). Without explicit, costly AIMD free energy simulations of liquid electrolyte outside the SEI film, we cannot determine which scenario is more likely. Fig. 6h explores the latter possibility by adding 12 Li atoms at the interface and 6 interstitial Li between the first two carbonate layers closest to the lithium surface. (Without the added 12 Li at the interface, the interstitial  $\text{Li}^+$  migrate on to the Li metal surface.) The charge distribution generates an initial voltage of about 0.5 V vs  $\text{Li}^+/\text{Li}(\text{s})$ . However, upon optimization, C-C linkages and four  $(\text{CO}_3)_2$  units are formed. This configuration is more favorable than Fig. 1e of this work by 0.08 eV per Li added after accounting for Li cohesive energy. It is unclear that a configuration with so many interstitials is kinetically assessable, and we consider this result speculative. Fig. 6h does emphasize the multitude of reactions  $\text{CO}_3^{2-}$  can undergo in this extremely electrochemically reductive environment, partly due to the large inherent instability associated with Eq. 1.

In the SI, we show that Si atoms substituting for Li on  $\text{Li}(100)$  surface reduces reactivity towards  $\text{Li}_2\text{CO}_3$ .  $\text{Li}_2\text{CO}_3$  decomposition on an amorphous-Si surface is also shown to be energetically unfavorable. To what extent  $\text{Li}_x\text{Si}$ , with finite Si content subsurface, will slow down this reaction will be the subject of future work.

## F. Interfacial Instability: AIMD Simulations Including Electrolyte

In this subsection, we consider the initial stages of SEI formation in a less well-controlled, liquid-solid interface environment, with LiF decorating the surface. LEDC instability has been demonstrated by Soto *et al.* on related surfaces.<sup>32</sup> Here AIMD simulations are conducted on a liquid electrolyte and a submonolayer of Li<sub>2</sub>VDC units on a Li<sub>13</sub>Si<sub>4</sub> surface coated with a 5-Å diameter LiF cluster (Fig. 1g-h). Li<sub>13</sub>Si<sub>4</sub> is chosen because of computational reasons; its unit cell exhibits better lattice matching with crystalline surface films.<sup>46</sup> The equilibrium voltage of this composition and the maximally lithiated Li<sub>22</sub>Si<sub>5</sub> has been predicted to differ by less than 0.1 V.<sup>96</sup> As discussed in the Introduction, Li<sub>2</sub>VDC may arise from vinylene carbonate decomposition, and is structurally similar to LEDC.

The outer layer of the thin SEI film is modeled by placing five Li<sub>2</sub>VDC oligomers on one side of the slab (Fig. 7). Li<sub>2</sub>VDC are placed in such a way that the whole surface is covered by the organic block. This corresponds to a coverage of approximately 1.77 oligomer/nm<sup>2</sup> based on the surface size. Therefore, our model mirrors an anode with a SEI layer formed by two components (LiF and Li<sub>2</sub>VDC) stacked perpendicular to the Li<sub>13</sub>Si<sub>4</sub> (010) surface slab. The liquid electrolyte region of the battery is placed on top of this surface. The electrolyte consists of pure FEC solvent molecules and 1.0 M LiPF<sub>6</sub> salt.

One Li<sub>2</sub>VDC molecule in contact with the open lithiated Si surface is found to decompose. Starting from the 2.5 ps step, a C<sub>carbonate</sub>-O<sub>vinylene</sub> bond breaks. The resulting OC<sub>2</sub>H<sub>2</sub>CO<sub>3</sub><sup>2-</sup> fragment remains adsorbed on the surface, with the O<sub>vinylene</sub> atom bonded with two Li<sub>surface</sub> atoms at an average distance of 1.80 Å, while the O<sub>carbonate</sub> atom is coordinated to a Li<sub>surface</sub> atom at a distance of 1.83 Å (Fig. 8a& b within the black dashed circles). A Bader charge analysis<sup>95</sup> reveals an almost neutral CO<sub>2</sub> molecule, which diffuses away from the surface, and an OCHCH<sub>2</sub> fragment bearing a negative charge (-1.79 |e|). The latter fragment is attached to the CO<sub>3</sub> group inside the red circle in Fig. 8. These AIMD simulations suggest that even Li<sub>2</sub>VDC oligomers, formed from electrolyte additive molecules, can be rapidly decomposed when in contact with active Li<sub>x</sub>Si anode surfaces decorated with LiF crystallites, in qualitative agreement with Ref. 32. Higher Li-content Li<sub>x</sub>Si are at lower voltage, and are expected to be even more reactive towards the SEI than Li<sub>13</sub>Si<sub>4</sub>.



## IV. DISCUSSIONS

The implications of this work are manifold. First, we stress that the interfacial reactivities predicted concern reactive anode material surfaces. We have not attempted SEI stability analysis on graphite interfaces herein. Even though LEDC and  $\text{Li}_2\text{CO}_3$  are always thermodynamically unstable at low voltages in the presence of excess Li, interfacial reactions (or other external means) must occur to trigger such instability. However, if lithium-plating occurs on the outer surfaces of SEI-covered graphite,<sup>47</sup> and this elemental lithium chemically decomposes the SEI there, our work predicts that organic SEI components, not just additional solvent molecules, may react rapidly there.

Extrapolating from our results, we speculate that Mn(II) and other transition metal ions diffusing to the anode surface may decompose organic SEI components via surface reactions on Mn metal surfaces and burn holes in the outer SEI layers. This may be one reason transition metal ions degrade passivating films.<sup>30,31</sup>

If the anode of interest is purely Li metal, our work suggests that different SEI components can decompose on its surface, releasing  $\text{O}^{2-}$  and carbon.  $\text{Li}_2\text{O}$  (and LiF, if a fluoride source is present) would be the passivating films covering the surface.  $\text{OC}_2\text{H}_4\text{O}^{2-}$  may also be present. However, Ref. 50 suggests that  $\text{OC}_2\text{H}_4\text{O}^{2-}$  rapidly reacts with intact solvent molecules to form oligomers that can subsequently yield  $\text{Li}_2\text{CO}_3$  and LEDC. Since the latter components are not stable on Li metal surfaces,  $\text{OC}_2\text{H}_4\text{O}^{2-}$  may eventually be destroyed in multistep reactions. The eventual thickness of the  $\text{Li}_2\text{O}$  oxide layer, and the fate of the small amount of carbon on the surface, depend on  $\text{O}^{2-}$  and  $\text{C}^{q-}$  diffusion rates inside Li metal, and will be the subjects of future studies.

The variations in reaction barriers for  $\text{Li}_2\text{CO}_3$  (001) with different amount of interfacial Li [Figs. 4d-e; Fig. 6h (zero barrier)], and for an isolated  $\text{CO}_3^{2-}$  (Fig. 4f), illustrate that the  $\text{Li}_2\text{CO}_3$  bond-breaking rate can strongly depend on the chemical environment. We have focused on the initial decomposition process, and speculate that, as  $\text{CO}_3^{2-}$  units are removed by reactions, they leave voids that can be filled by Li atoms, yielding more interstitials-like Li outcroppings that can accelerate decomposition of interfacial  $\text{CO}_3^{2-}$ . As  $\text{Li}_2\text{O}$  builds up at the interface, such reactions should be impeded. Note that other SEI components like  $\text{Li}_2\text{VDC}$  may still decompose on the outside of the  $\text{Li}_2\text{O}$  layer.<sup>32</sup>

If the anode is  $\text{Li}_x\text{Si}$ , the situation is more complex. LEDC films of varying thickness has

been shown in this work and elsewhere<sup>32</sup> to decompose on *both* Li(100) and  $\text{Li}_x\text{Si}$  surfaces.  $\text{Li}_2\text{CO}_3$  decomposition on  $\text{Li}_x\text{Si}$  is more challenging due to the possible surface modifications discussed in the previous paragraph. (See the S.I. for the effect of Si-atom doping the surface.) If  $\text{Li}_2\text{CO}_3$  also decomposes readily on  $\text{Li}_x\text{Si}$  surfaces, which we consider likely due to the fact that  $\text{Li}_x\text{Si}$  surfaces are covered with Li,<sup>46</sup>  $\text{O}^{2-}$  released from SEI components should form  $\text{Li}_2\text{O}$  during charging (see experimental evidence discussed below). Upon discharge,  $\text{Li}_x\text{Si}_y\text{O}_z$  becomes thermodynamically favored over  $\text{Li}_2\text{O}$ .<sup>97</sup> Hence there could be some transfer of oxygen from the SEI to silicon. It is unclear whether the possibly small amount of carbon released from SEI products forms graphite or remains lithium carbide. The initial  $\text{SiO}_2$  covering the Si surface should transform into lithium silicate phases at low voltages.<sup>97</sup> It is uncertain whether  $\text{Li}_x\text{Si}_y\text{O}_z$  formation is fully reversible.<sup>98</sup>

X-ray photoemission spectroscopy (XPS), with varying photon energies,<sup>18–20</sup> and time-of-flight secondary ion spectroscopy,<sup>7</sup> have been used to perform depth profiling of the SEI.  $\text{Li}_2\text{O}$  has been found in the SEI region immediately next to  $\text{Li}_x\text{Si}$  in silicon anodes, although this has been attributed to the transformation of  $\text{SiO}_2$ .<sup>18,19</sup> This  $\text{Li}_2\text{O}$  slowly transforms into LiF, indicating that even the deepest-lying SEI layer can undergo evolution as cycling proceeds.<sup>18,19</sup> Since we have not considered F-containing compounds in our static DFT work, the competition between LiF and  $\text{Li}_2\text{O}$  in the innermost SEI layer will be the subject of future studies. We also note that  $\text{Li}_2\text{O}$  is unstable with respect to electron beams and moisture. Regarding  $\text{Li}_2\text{CO}_3$  decomposition, electrochemical reduction of this species has recently been demonstrated under restricted conditions.<sup>80</sup> A promising approach to pinpoint SEI reactions on the immediate surfaces of active electrode materials may be UHV-based measurements.<sup>49</sup>

Our demonstration of LEDC instability on Li metal surfaces is another reason that the inner SEI films on  $\text{Li}_x\text{Si}$  and Li(s) consists only of inorganic components and the outer region contains organic compounds. It is possible that organic components may coat on the electrode surface after first nucleating in the liquid electrolyte region,<sup>99</sup> and then transform into inorganic components like  $\text{Li}_2\text{O}$ . In light of this work, it is of interest to re-examine the stability of newly discovered SEI components.<sup>100</sup>

We stress that most calculations in this work are either static or short AIMD trajectories. Our simulation conditions can only be related to dynamical measurements qualitatively. For example, the charging or “C”-rate cannot be quantified. However, quasi-static overpotential voltage conditions can be represented by creating mismatches between the electronic

voltage (related to Fermi levels) and ionic voltage (related to lithium content).<sup>51</sup> In anode materials like Si or Sn, SEI thickness and chemical composition (e.g., organic vs. inorganic) can change during charge/discharge; the passivating film can even crack, exposing pristine anode materials, and needs to be reformed from scratch (i.e., the surfaces are at “zero SEI thickness”). DFT-based data will be crucial to parameterize multiscale models to address these issues.

Finally, in terms of modeling, this work highlights the challenges facing systematic treatment of buried solid-solid interfaces.<sup>33,34,36,37</sup> Imaging techniques have yet to achieve the resolution needed to elucidate the atomic details that can be used as starting points for modeling such interfaces. Therefore a suite of surface models ranging from pristine to defect-incorporated are considered. Other factors to be considered in the future include strain induced by inserting/removal Li during charge/discharge. The low bulk modulus Li metal and high “x”  $\text{Li}_x\text{Si}$  materials considered in this work are not expected to have their electronic properties or reactivities strongly affected by strain, but amorphous Si may. Chemical/spatial heterogeneities, facet dependence, and mechanical deformation also need to be addressed. Systematization of interfacial modeling will likely emerge after more modeling studies of individual sets of interfaces have highlighted the commonalities and differences.

## V. CONCLUSIONS

In this work, we consider three criteria of SEI stability: thermodynamic, electrochemical, and interfacial. Two key SEI components, lithium carbonate ( $\text{Li}_2\text{CO}_3$ ) and lithium ethylene dicarbonate (LEDC), are predicted to be electrochemically stable but thermodynamically unstable. The fundamental reason for thermodynamic instability is likely the existence of carbon atoms in high formal charge states under highly electrochemically reductive conditions. By this definition, we conjecture that most carbon-containing SEI components may actually be thermodynamically unstable.

Interfacial reactions can trigger the decomposition of these SEI products. Our static DFT calculations focus on the interfaces between these SEI components and two model surfaces. Li(100) and a-Si are chosen to represent two extremes of reactive anode. LEDC proves to be fragile, decomposing on Li(100) with reaction barriers predicted to be significantly lower than 0.92 eV. This suggests that decomposition will occur within battery operation (i.e.,

about one-hour) timescales. LEDC decomposition on a-Si surfaces is predicted to be slower than the 1-hour threshold time frame.  $\text{Li}_2\text{CO}_3$  decomposition is observed on Li metal surfaces. The reaction barrier is below the 0.92 eV threshold in the presence of excess Li atoms at the interface. Therefore we predict that a thin layer of  $\text{Li}_2\text{O}$ , of at present unknown thickness, exists on lithium metal surfaces below the rest of the SEI components, unless  $\text{Li}_2\text{O}$  is subsequently converted into LiF. Similar  $\text{Li}_2\text{CO}_3$  degradation reactions and  $\text{Li}_2\text{O}$  formation are speculated to occur on high Li-content  $\text{Li}_x\text{Si}$  surfaces. DFT-based molecular dynamics simulations are also used to demonstrate that organic SEI components spontaneously decomposes on explicit  $\text{Li}_x\text{Si}$  surfaces. Carboxide groups are found to be kinetically stable in the absence of liquid electrolytes. Our predictions have multiple implications for SEI evolution during cycling on Li metal and Si anodes, and undesirable Li-plating on the SEI.

### Acknowledgement

We thank Oleg Borodin, Byron Konstantinos Antonopoulos, Wentao Song, and Janice Reutt-Robey for discussions and input. Sandia National Laboratories is a multiprogram laboratory managed and operated by Sandia Corporation, a wholly owned subsidiary of Lockheed Martin Corporation, for the U.S. Department of Energy's National Nuclear Security Administration under contract DE-AC04-94AL85000. This work was supported by the Assistant Secretary for Energy Efficiency and Renewable Energy, Office of Vehicle Technologies of the U. S. Department of Energy under Contract No. DE-AC02-05CH11231, Subcontract No. 7060634 under the Advanced Batteries Materials Research (BMR) Program.

---

<sup>1</sup> *Advances in lithium-ion batteries*, edited by van Schalkwijk, W.A. & Scrosati, B. (Kluwer, New York, 2002).

<sup>2</sup> Jow, T.R.; Xu, K.; Borodin, O.; Ue, Makoto, ed. *Electrolytes for Lithium and Lithium-Ion Batteries* (Springer, 2014)

<sup>3</sup> *Lithium-ion batteries: solid-electrolyte interphase*, edited by Wang Y.; Balbuena P.B. (Imperial College, London, 2004).

- <sup>4</sup> Xu, K. Electrolytes and Interphases in Li-Ion Batteries and Beyond. *Chem. Rev.* **2014**, *114*, 11503-11618.
- <sup>5</sup> Verma, P.; Maire, P.; Novák, P. A Review of the Features and Analyses of the Solid Electrolyte Interphase in Li-ion Batteries. *Electrochim. Acta* **2010**, *55*, 6332-6341.
- <sup>6</sup> Aurbach, D.; Gofer, Y.; Ben-Zion, M.; Aped, P. The Behavior of Lithium Electrodes in Propylene and Ethylene Carbonate: the Major Factors that Influence Li Cycling Efficiency. *J. Electroanal. Chem.* **339**, 451 (1992).
- <sup>7</sup> Lu, P.; Li, C.; Schneider, E.W.; Harris, S.J. Chemistry, Impedance, and Morphology Evolution in Solid Electrolyte Interphase Films during Formation in Lithium Ion Batteries. *J. Phys. Chem. C* **2014**, *118*, 896-903.
- <sup>8</sup> Tang, M.; Miyazaki, K.; Abe, T.; Newman, J. Effect of Graphite Orientation and Lithium Salt on Electronic Passivation of Highly Oriented Pyrolytic Graphite. *J. Electrochem. Soc.* **2012**, *159* A634-A641.
- <sup>9</sup> Zhu, Z.; Zhou, Y.; Vemuri, R.S.; Xu, W.; Zhao, R.; Wang, X.; Thevuthasan, S.; Baer, D.R.; Wang, C.-M. In-situ Mass Spectrometric Determination of Molecular Structural Evolution at the Solid Electrolyte Interphase in Lithion-Ion Batteries. *Nano Lett.* **2015** *15*, 6170-6176.
- <sup>10</sup> Arreaga-Salas, D.E.; Sra, A.K.; Roodenko, K.; Chabal, Y.J.; Hinkle, C.L. Progression of Solid Electrolyte Interphase Formation on Hydrogenated Amorphous Silicon Anodes for Lithium-Ion Batteries. *J. Phys. Chem. C* **2012**, *116*, 9072 (2012).
- <sup>11</sup> Zhang, W.-J. A Review of the Electrochemical Performance of Alloy Anodes for Lithium-ion Batteries. *J. Power Sources* **2011**, *196*, 13-24.
- <sup>12</sup> Chan, C.K.; Ruffo, R.; Hong, S.S.; Cui, Y. Surface Chemistry and Morphology of the Solid Electrolyte Interphase on Silicon nanowire Lithium-Ion Battery Anodes. *J. Power Sources* **2009**, *189*, 1132-1140.
- <sup>13</sup> Ruffo, R.; Hong, S.S.; Chan, C.K.; Huggins, R.A., Cui, Y. Impedance Analysis of Silicon Nanowire Lithium Ion Battery Anodes. *J. Phys. Chem. C* **2009**, *113*, 11390-11398.
- <sup>14</sup> Kim, T.; Park, S.; Oh, S.M. Solid-state NMR and Electrochemical Dilatometry Study on Li<sup>+</sup> Uptake/Extraction Mechanism in SiO Electrode. *J. Electrochem. Soc.* **2007**, *154*, A1112-A1117.
- <sup>15</sup> Etacheri, V.; Haik, O.; Gofer, Y.; Roberts, G.A.; Stefan, I.C.; Fasching, R.; Aurbach, D. Effect of Fluoroethylene Carbonate (FEC) on the Performance and Surface Chemistry of Si-Nanowire

- Li-ion Battery Anodes. *Langmuir*, **2012**, *28*, 965-976.
- <sup>16</sup> Zhang, B.; Metzger, M.; Solchenbach, S.; Payne, M.; Meini, S.; Gasteiger, H.A.; Garsuch, A.; Lucht, B.L. Role of 1,3-Propane Sultone and Vinylene Carbonate in Solid Electrolyte Interphase Formation and Gas Generation. *J. Phys. Chem. C* **2015**, *119*, 11337-11348.
- <sup>17</sup> Nie, M.; Abraham, D.P.; Chen, Y.; Bose, A.; Lucht, B.L. Silicon Solid Electrolyte Interphase (SEI) of Lithium Ion Battery Characterized by Microscopy and Spectroscopy. *J. Phys. Chem. C* **2013**, *117*, 13403-13412.
- <sup>18</sup> Philippe, B.; Dedryvere, R.; Gorgoi, M.; Rensmo, H.; Gonbeau, D.; Edström K. Role of the LiPF<sub>6</sub> Salt for the Long-Term Stability of Silicon Electrodes in Li-Ion Batteries – a Photoelectron Spectroscopy Study. *Chem. Mater.* **2013**, *25*, 394-404.
- <sup>19</sup> Philippe, B.; Dedryvere, R.; Gorgoi, M.; Rensmo, H.; Gonbeau, D.; Edström K. Improved Performances of Nanosilicon Electrodes using the Salt LiFSI: A Photoelectron Spectroscopy Study. *J. Am. Chem. Soc.* **2013**, *135*, 9829-9842.
- <sup>20</sup> Xu, C.; Lindgren, F.; Philippe, B.; Gorgoi, M.; Björefors, F.; Edström K; Gustafsson, T. Improved Performance of the Silicon Anode for Li-ion Batteries: Understanding the Surface Modification Mechanism of Fluoroethylene Carbonate as an Effective Electrolyte Additive. *Chem. Mater.* **2015**, *27*, 2591-2599
- <sup>21</sup> Lee, S.W.; McDowell, M.T.; Berla, L.A.; Nix, W.D.; Cui, Y. Fracture of Crystalline Silicon Nanopillars during Electrochemical Lithium Insertion. *Proc. Natl. Acad. Sci.* **2012**, *109*, 4080-4085.
- <sup>22</sup> Zhang, L.Q.; Liu, X.H.; Liu, Y.; Huang, S.; Zhu, T.; Gui, L.; Mao, S.X.; Ye, Z.Z.; Wang, C.M.; Sullivan, J.P.; Huang, J.Y. Controlling the Lithiation-Induced Strain and Charging Rate in Nanowire Electrodes by Coating. *ACS Nano* **2011**, *5*, 4800-4809.
- <sup>23</sup> Aurbach, D.; Daroux, M.; McDougall, G.; Yeager, E.B. Spectroscopic Studies of Lithium in an Ultrahigh-vacuum System. *J. Electroanal. Chem.*, **1993**, *358*, 63-76.
- <sup>24</sup> Schechter, A.; Aurbach, D.; Cohen, H. X-ray Photoelectron Spectroscopy Study of Surface Films Formed on Li Electrodes Freshly Prepared in Alkyl Carbonate Solutions. *Langmuir*, **1999**, *15*, 3334-3342.
- <sup>25</sup> Xu, W.; Wang, J.; Ding, F.; Chen, X.; Nasybulin, E.; Zhang, Y.; Zhang, J.-G. Lithium Metal Anodes for Rechargeable Batteries. *Energy Envir. Sci.* **2014**, *7*, 513-537.
- <sup>26</sup> Tasaki, K.; Harris, S.J. Computational Study on the Solubility of Lithium Salts Formed on

- Lithium Ion battery Negative Electrode in Organic Solvents. *J. Phys. Chem. C* **2010**, *114*, 8076-8083.
- <sup>27</sup> Lee, H.H.; Wan, C.C.; Wang, Y.Y. Thermal Stability of the Solid Electrolyte Interface on Carbon Electrodes of Lithium Batteries. *J. Electrochem. Soc.* **2004**, *151*, A542-A547.
- <sup>28</sup> Park, H.; Yoon, T.; Mun, J.; Ryu, J.H.; Kim, J.J.; Oh, S.M. A Comparative Study on Thermal Stability of Two Solid Electrolyte Interphase (SEI) Films on Graphite Negative Electrode. *J. Electrochem. Soc.* **2013**, *160*, A1539-A1543.
- <sup>29</sup> Choo, M.-H.; Nguyen, C.C.; Hong, S.; Kwon, Y.H.; Woo, S.-W.; Kim, J.Y.; Song, S.-W. Combination of Acid-resistor and -Scavenger Improves the SEI Stability and Cycling Ability of Tinnickel Battery Anodes in LiPF<sub>6</sub>-containing Electrolyte. *Electrochim. Acta* **2013**, *112*, 252-257.
- <sup>30</sup> Joshi, T.; Eom, K.; Yushin, G.; Fuller, T.F. Effects of Dissolved Transition Metals on the Electrochemical Performance and SEI Growth in Lithium-Ion Batteries. *J. Electrochem. Soc.* **2014**, *161*, A1915-A1921.
- <sup>31</sup> Shkrob, I.A.; Kropf, A.J.; Marin, T.W.; Li, Y.; Poluektov, O.G.; Niklas, J.; Abraham, D.P. Manganese in Graphite Anode and Capacity Fade in Li Ion Batteries. *J. Phys. Chem. C* **2014**, *118*, 24335-24348.
- <sup>32</sup> Soto, F.; Ma, Y.; Martinez de la Hoz, J.; Seminario, J.; Balbuena, P. Formation and Growth Mechanisms of Solid-Electrolyte Interphase Layers in Rechargeable Batteries. *Chem. Mater.* **2015**, *27*, 7990-8000.
- <sup>33</sup> Haruyama, J.; Sodeyama, K.; Han, L.; Takada, K.; Tateyama, Y. Space-Charge Layer Effect at Interface between Oxide Cathode and Sulfide Electrolyte in All-Solid-State Lithium-Ion Battery. *Chem. Mater.* **2014**, *26*, 4248-4255.
- <sup>34</sup> Lepley, N.D.; Holzwarth, N.A.W. Modeling Interfaces Between Solids: Application to Li Battery Materials. *Phys. Rev. B* (to appear).
- <sup>35</sup> Lepley, N.D.; Holzwarth, N.A.W.; Du, Y.A. Structures, Li<sup>+</sup> Mobilities, and Interfacial Properties of Solid Electrolytes Li<sub>3</sub>PS<sub>4</sub> and Li<sub>3</sub>PO<sub>4</sub> from First Principles. *Phys. Rev. B* **2013**, *88*, 104103.
- <sup>36</sup> Santosh, K.C.; Xiong, K.; Longo, R.C.; Cho, K. Interfacial Phenomena between Li Anode and Lithium Phosphate Electrolyte for Li-ion Battery. *J. Power Sources* **2013**, *244*, 136-142.
- <sup>37</sup> Sumita, M.; Tanaka, Y.; Ikeda, M.; Ohno, T. Theoretically Designed Li<sub>3</sub>PO<sub>4</sub> (100)/LiFePO<sub>4</sub>

- (010) Coherent Electrolyte/Cathode Interface for All Solid-State Li Ion Secondary Batteries. *J. Phys. Chem. C* **2015**, *119*, 14-22.
- <sup>38</sup> Ong, S.P.; Andreussi, O.; Wu, Y.; Marzari, N.; Ceder, G. Electrochemical Windows of Room-Temperature Ionic Liquids from Molecular Dynamics and Density Functional Theory Calculations. *Chem. Mater.* **2011**, *23*, 2979-2986.
- <sup>39</sup> Mo, Y.; Ong, S.P.; Ceder, G. First Principles Study of the  $\text{Li}_{10}\text{GeP}_2\text{S}_{12}$  Lithium Super Ionic Conductor Material. *Chem. Commun.* **2012**, *24*, 15-17.
- <sup>40</sup> Zhu, Y.Z.; He, X.F.; Mo, Y.F. Origin of Outstanding Stability in the Lithium Solid Electrolyte Materials: Insights from Thermodynamic Analyses Based on First-Principles Calculations. *ACS Appl. Mater. Interfaces* **2015**, *7*, 23685-23693.
- <sup>41</sup> Ong, S.P.; Mo, Y.; Richards, W.D.; Miara, L.; Lee, H.S.; Ceder, G. Phase Stability, Electrochemical Stability, and Ionic Conductivity of the  $\text{Li}_{10\pm 1}\text{MP}_2\text{X}_{12}$  (M=Ge, Si, Sn, Al or P, and X-O, S or Se) Family of Superionic Conductors. *Energy Environ. Sci.* **2013**, *6*, 148-156.
- <sup>42</sup> Borodin, O.; Olguin, M.; Spear, C.E.; Leiter, K.W.; Knap, J. Towards High Throughput Screening of Electrochemical Stability of Battery Electrolytes. *Nanotech.* **2015**, *26*, 354003.
- <sup>43</sup> Goodenough, J.B.; Park, K.-S. The Li-Ion Rechargeable Battery: A Perspective. *J. Am. Chem. Soc.*, **2013**, *135*, 1167-1176.
- <sup>44</sup> Gauthier, M.; Carney, T.J.; Grimaud, A.; Giodano, L.; Pour, N.; Chang, H.H.; Fenning, D.P.; Lux, S.F.; Paschos, O.; Bauer, C.; Magia, F.; Lupart, S.; Lamp, P.; Shao-Horn, Y. Electrode-Electrolyte Interface in Li-Ion Batteries: Current Understanding and New Insights. *J. Phys. Chem. Lett.* **2015**, *6*, 4653-4672.
- <sup>45</sup> Perez-Beltran, S.; Ramirez-Caballero, G.E.; Balbuena, P.B. First-Principles Calculations of Lithiation of a Hydroxylated Surface of Amorphous Silicon Dioxide. *J. Phys. Chem. C* **2015**, *119*, 16424-16431.
- <sup>46</sup> Leung, K.; Rempe, S.B.; Foster, M.E.; Ma, Y.; Martinez de la Hoz, J.M.; Sai, N.; Balbuena, P.B. Modeling Electrochemical Decomposition of Fluoroethylene Carbonate on Silicon Anode Surfaces in Lithium Ion Batteries *J. Electrochem. Soc.*, **2014**, *161*, A213-A221.
- <sup>47</sup> Zinth, V.; von Lüders, C.; Hofmann, M.; Hattendorff, J.; Buchberger, I.; Erhard, S.; Rebelo-Kornmeier, J.; Jossen, A.; Gilles, R. Lithium Plating in Lithion-ion Batteries at Sub-ambient Temperatures Investigated by in-situ Neutron Diffraction. *J. Power Sources* **2014**, *271*, 152-159.



- <sup>48</sup> Li, Z.; Huang, J.; Liaw, B.Y.; Metzler, V.; Zhang, J. A Review of Lithium Deposition in Lithium-ion and Lithium Metal Secondary Batteries. *J. Power Sources* **2014**, *254*, 168-182.
- <sup>49</sup> Song, W.; Bharath, S.; Reutt-Robey, J. Adsorption and Reaction Branching of Molecular Carbonates on Lithiated C(0001) Substrates. *J. Phys. Chem. C* **2014**, *118*, 19017-19022.
- <sup>50</sup> Leung, K. Two-electron Reduction of Ethylene Carbonate: a Quantum Chemistry Re-examination of Mechanisms. *Chem. Phys. Lett.* **2013**, *568-569*, 1-8.
- <sup>51</sup> Leung, K.; Leenheer, A. How Voltage Drops are Manifested by Lithium Ion Configurations at Interfaces and in Thin Films on Battery Electrodes. *J. Phys. Chem. C* **2015**, *119*, 10234-10246.
- <sup>52</sup> Cheng, J.; Sprik, M. Alignment of Electronic Energy Levels at Electrochemical Interfaces. *Phys. Chem. Chem. Phys.* **2012**, *14*, 11245-11267.
- <sup>53</sup> Schnur, S.; Gross, A. Properties of Metal-Water Interfaces Studied from First Principles. *New J. Phys.* **2009**, *11*, 125003.
- <sup>54</sup> Taylor, C.D.; Wasileski, S.A.; Filhol, J.-S.; Neurock, M. First Principles Reaction Modeling of the Electrochemical Interface: Consideration and Calculation of a Tunable Surface Potential From Atomic and Electronic Structure. *Phys. Rev. B* **2006**, *73*, 165402.
- <sup>55</sup> Nielsen, M.; Björketun, M.E.; Hansen, M.H.; Rossmeisl, J. Towards First Principles Modeling of Electrochemical Electrode-Electrolyte Interfaces. *Sur. Sci.* **2015**, *631*, 2-7.
- <sup>56</sup> D. Opalka, T.A. Pham, M. Sprik, and G. Galli, *J. Chem. Phys.*, 2014, **141**, 034501.
- <sup>57</sup> Bonnet, N.; Morishita, T.; Sugino, O.; Otani, M. First-Principles Molecular Dynamics at a Constant Electrode Potential. *Phys. Rev. Lett.* **2012**, *109*, 266101.
- <sup>58</sup> Letchworth-Weaver, K.; Arias, T. A. Joint Density Functional Theory of the Electrode-electrolyte Interface: Application to Fixed Electrode Potentials, Interfacial Capacitances, and Potentials of Zero Charge. *Phys. Rev. B* **2012**, *96*, 075140.
- <sup>59</sup> Kharche, N.; Muckerman, J.T.; Hybertsen, M.S. First-Principles Approach to Calculating Energy Level Alignment at Aqueous Semiconductor Interfaces. *Phys. Rev. Lett.* **2014**, **113**, 176802.
- <sup>60</sup> Tavassol, H.; Chan, M.K.Y.; Catarello, M.G.; Greeley, J.P. Cahill, D.G.; Gewirth, A.A. Surface Coverage and SEI Induced Electrochemical Surface Stress Changes during Li Deposition in a Model System for Li-Ion Battery Anodes *J. Electrochem. Soc.* **2013**, *160*, A888-A896.
- <sup>61</sup> Chou, C.-Y.; Hwang, G.S. Surface Effects on the Structure and Lithium Behavior in Lithiated Silicon: A First Principles Study. *Sur. Sci.* **2013**, *612*, 16-23.

- <sup>62</sup> Kresse, G.; Furthmüller, J. Efficient Iterative Schemes for Ab Initio Total-Energy Calculations Using a Plane-wave Basis Set. *Phys. Rev. B* **1996**, *54*, 11169.
- <sup>63</sup> Kresse, G.; Joubert, J. From Ultrasoft Pseudopotentials to the Projector Augmented-Wave Method. *Phys. Rev. B* **1999**, *59*, 1758-1775.
- <sup>64</sup> Paier, J.; Marsman, M.; Kresse, G. Why does the B3LYP hybrid functional fail for metals? *J. Chem. Phys.* **2007**, *127*, 024103.
- <sup>65</sup> Perdew, J.P.; Burke, K.; Ernzerhof, M. Generalized Gradient Approximation Made Simple. *Phys. Rev. Lett.* **1996**, *77*, 3865-3868.
- <sup>66</sup> Heyd, J.; Scuseria, G.E.; Ernzerhof, M. Hybrid Functionals based on a Screened Coulomb Potential. *J. Chem. Phys.* **2003**, *118*, 8207-8215; *ibid.*, **2006**, *124*, 219906; *J. Chem. Phys.*, Vydrov, O.A.; Heyd, J.; Krukau, A.V.; Scuseria, G.E. Assessment of a Long-range Corrected Hybrid Functional. **2006**, *125*, 074106.
- <sup>67</sup> Mori-Sanchez, P.; Cohen, A.J.; Yang W.T. Localization and Delocalization Errors in Density Functional Theory and Implications for Band-gap Prediction. *Phys. Rev. Lett.* **2008**, *100*, 146401.
- <sup>68</sup> Martinez de la Hoz, J.M.; Balbuena, P.B. Reduction Mechanisms of Additives on Si Anodes of Li-Ion Batteries. *Phys. Chem. Chem. Phys.* **2014**, *16*, 17091-10798.
- <sup>69</sup> Henkelman, G.; Uberuaga, B.P.; Jonsson, H. A Climbing Image Nudged Elastic Band Method for Finding Saddle Points and Minimum Energy Paths. *J. Chem. Phys.* **2000**, *113*, 9901-9985.
- <sup>70</sup> Neugebauer, J.; Scheffler, M. Adsorbate-substrate and Adsorbate-adsorbate Interactions of Na and K adlayers on Al(111). *Phys. Rev. B* **1992**, *46*, 16067-16080.
- <sup>71</sup> Chan, M.K.Y.; Long, B.R.; Gewirth, A.A.; Greeley, J.P. The First-Cycle Electrochemical Lithiation of Crystalline Ge: Dopant and Orientation Dependence and Comparison with Si. *J. Phys. Chem. Lett.* **2011**, *2*, 3092-3095.
- <sup>72</sup> Accelrys Software Inc., D.S.M.E., Release 4.0, San Diego: Accelrys Software Inc., 2013.
- <sup>73</sup> Grazulis, S.; Chateigner, D.; Downs, R.T.; Yokochi, A.F.T.; Quiros, M.; Lutterotti, L.; Manakova, E.; Butkus, J.; Moeck, P.; Le Bail, A.: Crystallography Open Database – an open-access collection of crystal structures. *J. Appl. Cryst.* **2009**, *42*, 726-729.
- <sup>74</sup> Casewit, C.J.; Colwell, K.S.; Rappe, A.K. Application of a Universal Force Field to Organic Molecules. *J. Am. Chem. Soc.* **1992**, *114*, 10035-10046.
- <sup>75</sup> Gaussian 09, Revision A.1, M.J. Frisch *et al.*, Gaussian, Inc., Wallingford CT, 2009.

- <sup>76</sup> Ernzerhof, M.; Scuseria, G.E. Assessment of the Perdew-Burke-Ernzerhof exchange-correlation functional *J. Chem. Phys.* **1999**, *110*, 5029-5036; Adamo, C.; Barone, V.; Toward Reliable Density Functional Methods without Adjustable parameters: The PBE0 Model. *J. Chem. Phys.* **1999**, *110*, 6158-6170.
- <sup>77</sup> Marenich, A.V.; Cramer, C.J.; Truhlar, D.G. *J. Phys. Chem. B* Universal Solvation Model Based on Solute Electron Density and on a Continuum Model of the Solvent Defined by the Bulk Dielectric Constant and Atomic Surface Tensions. **2009**, *113*, 6378-6396.
- <sup>78</sup> Duan, Y.; Sorescu, D.C. Density Functional Theory Studies of the Structural, Electronic, and Phonon Properties of Li<sub>2</sub>O and Li<sub>2</sub>CO<sub>3</sub>: Application to CO<sub>2</sub> Capture Reaction. *Phys. Rev. B* **2009**, *79*, 014301.
- <sup>79</sup> Borodin, O.; Bedrov, D. Interfacial Structure and Dynamics of the Lithium Alkyl Dicarboxylate SEI Components in Contact with the Lithium Battery Electrolyte. *J. Phys. Chem. C* **2014**, *118*, 18362-18371.
- <sup>80</sup> Tian, N.; Hua, C.; Wang, Z.; Chen, L.Q. Reversible Reduction of Li<sub>2</sub>CO<sub>3</sub>. *J. Chem. Mater. A* **2015**, *3*, 14173-14177, and references therein.
- <sup>81</sup> Yu, J.M.; Balbuena, P.B.; Budzien, J.L.; Leung, K. Hybrid DFT Functional-based Static and Molecular Dynamics Studies of Excess Electron in Liquid Ethylene Carbonate *J. Electrochem. Soc.* **2011**, *158*, A400-410.
- <sup>82</sup> Garcia-Lastra, J.M.; Myrdal, J.S.G.; Christensen, R.; Thygesen, K.S.; Vegge, T. DFT+U Study of Polaronic Conduction in Li<sub>2</sub>O<sub>2</sub> and Li<sub>2</sub>CO<sub>3</sub>: Implications for Li-Air Batteries. *J. Phys. Chem. C* **2013**, *117*, 5568-5577.
- <sup>83</sup> A previous work on crystalline Li<sub>2</sub>CO<sub>3</sub> finds that adding e<sup>-</sup> and Li<sup>+</sup> interstitial (i.e., a Li atom) constitute a low-energy defect under battery operating conditions.<sup>84</sup> For the purpose of estimated reduction potential, we have not considered interstitials.
- <sup>84</sup> Shi, S.; Qi, Y.; Li, H.; Hector, L.G. Defect Thermodynamics and Diffusion Mechanisms in Li<sub>2</sub>CO<sub>3</sub> and Implications for the Solid Electrolyte Interphase in Li-Ion Batteries. *J. Phys. Chem. C* **2013**, *117*, 8579-8593.
- <sup>85</sup> The release of "CO<sub>2</sub>" should not be considered oxidation. CO<sub>2</sub> molecules are electrochemically reduced at ~ -2 V vs. SHE (~ 1 V vs. Li<sup>+</sup>/Li(s)) in organic solvents.<sup>86</sup>
- <sup>86</sup> Fujita, E. Photochemical Carbon Dioxide Reduction with Metal Complexes. *Coord. Chem. Rev.* **1999**, *185*, 373-384.

- <sup>87</sup> Tavassol, H.; Buthker, J.W.; Ferguson, G.A.; Curtiss, L.A.; Gewirth, A.A. Solvent Oligomerization during SEI Formation on Model Systems for Li-Ion Battery Anodes. *J. Electrochem. Soc.* **2012**, *159*, A730-A738.
- <sup>88</sup> Shkrob, I.A.; Wishart, J.F.; Abraham, D.P. What Makes Fluoroethylene Carbonate Different? *J. Phys. Chem. C* **2015**, *119*, 14954-14964.
- <sup>89</sup> Browning, K.L.; Baggetto, L.; Unocic, R.R.; Dudney, N.J.; Veith, G.M. Gas Evolution from Cathode Materials: a Pathway to Solvent Decomposition ConComitant to SEI Formation. *J. Power Sources* **2013**, *239*, 341-346.
- <sup>90</sup> Togasaki, N.; Momma, T.; Osaka, T. Role of the Solid Electrolyte Interphase on a Li Metal Anode in a Dimethylfulfoxide-based Electrolyte for a Lithium-oxygen Battery. *J. Power Sources* **2015**, *294*, 588-592.
- <sup>91</sup> Gachot, G.; Grugeon, S.; Armand, M.; Pilard, S.; Guenot, P.; Tarascon, J.M.; Laruelle, S. Deciphering the Multi-step Degradation Mechanisms of Carbonate-based Electrolyte in Li Batteries. *J. Power Sources* **2008**, *178*, 409-421.
- <sup>92</sup> We have considered displacing the  $\text{Li}_2\text{CO}_3$  and the Li(100) slabs relative to each other in the lateral directions. The entire  $\text{Li}_2\text{CO}_3$  slab is moved in the  $x$ - or  $y$ -directions by increments of 1 Å, and the geometry is optimized. The resulting energy change per surface  $\text{Li}_2\text{CO}_3$  formula unit is small, in the range  $-0.01$  to  $0.034$  eV.
- <sup>93</sup> In constast, in the LEDC simulation cells of Fig. 3, the  $\text{C}_2\text{H}_4$  backbones are exposed to the surface. Organic solvents will exhibit far less preferential orientations on this surface and their effects on the electronic voltage will be less than on  $\text{Li}_2\text{CO}_3$  surfaces.
- <sup>94</sup> Reactive force field-based molecular dynamics simulations have predicted  $\text{Li}_2\text{O}$  formation from  $\text{CO}_3^{2-}$ , although Li atom injection into the SEI region is needed; no spontaneous reaction is observed for  $\text{Li}_2\text{CO}_3$  on lithium metal surfaces. See: Kim, S.-P.; van Duin, A.C.T.; Shenoy, V.B. Effect of Electrolytes on the Structure and Evolution of the Solid Electrolyte Interphase (SEI) in Li-ion Batteries: a Molecular Dynamics Study. *J. Power Sources* **2011**, *196*, 8590-8597.
- <sup>95</sup> Henkelman, G.; Arnaldsson, A.; Jónsson, H. A Fast and Robust Algorithm for Bader Decomposition of Charge Density. *Comput. Mater. Sci.* **2006**, *36*, 354-360.
- <sup>96</sup> Chevrier, V.L.; Zwanziger, J.W.; Dahn, J.R. First Principles Study of Li-Si Crystalline Phases: Charge Transfer, Electronic Structure, and Lattice Vibrations. *J. Alloys Compounds* **2010**, *496*, 25-36.

- <sup>97</sup> Kim, S.-Y.; Qi, Y. Property Evolution of Al<sub>2</sub>O<sub>3</sub> Coated and Uncoated Si Electrodes: A First Principles Investigation. *J. Electrochem. Soc.* **2014**, *161*, F3137-F3143.
- <sup>98</sup> Hubaud, A.A.; Yang, Z.Z.; Schroeder, D.J.; Dogan, F.; Trahey, L.; Vaughrey, J.T. Interfacial Study of the Role of SiO<sub>2</sub> on Si Anodes Using Electrochemical Quartz Crystal Microbalance. *J. Power Sources* **2015**, *282*, 639-644.
- <sup>99</sup> Ushirogata, K.; Sodeyama, K.; Futera, Z.; Tateyama, Y.; Okuno, Y. Near Shore Aggregation Mechanism of Electrolyte Decomposition Products to Explain Solid Electrolyte Interphase Formation. *J. Electrochem. Soc.* **2015**, *162*, A2670-A2678.
- <sup>100</sup> See, e.g., Leifer, N.; Smart, M.C.; Parkash, G.K.S.; Gonzalez, L.; Sanchez, L.; Smith, K.A.; Bhalla, P.; Grey, C.P.; Greenbaum, S.G. <sup>13</sup>C Solid State NMR Suggests Unusual Breakdown Products in SEI Formation on Lithium Ion Electrodes. *J. Electrochem. Soc.* **2011**, *158*, A471-A480.

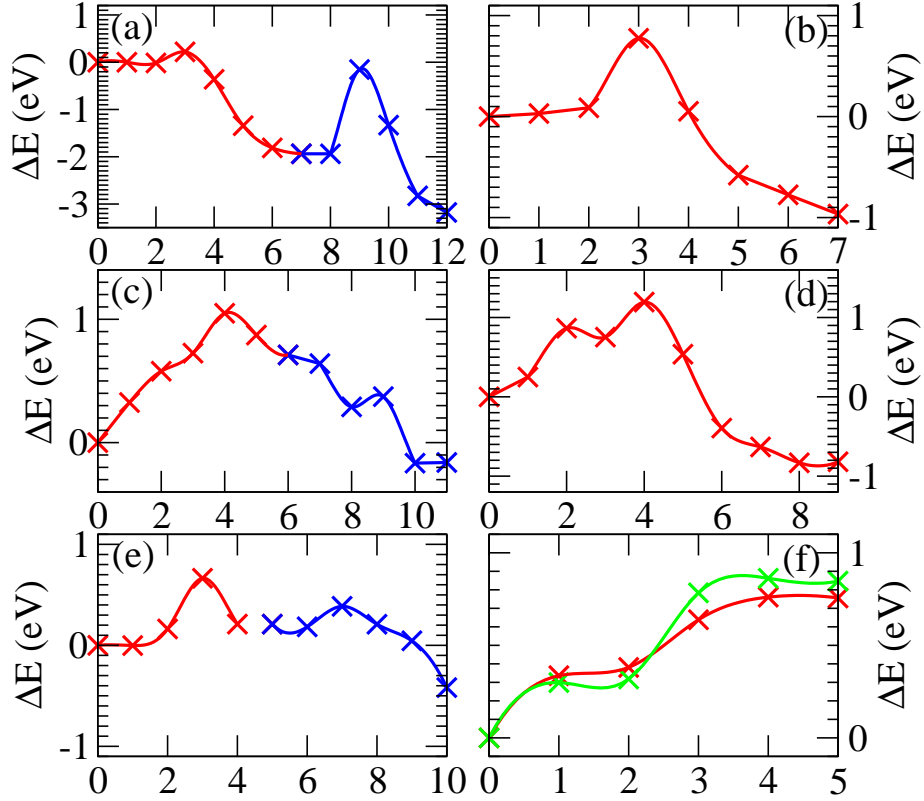
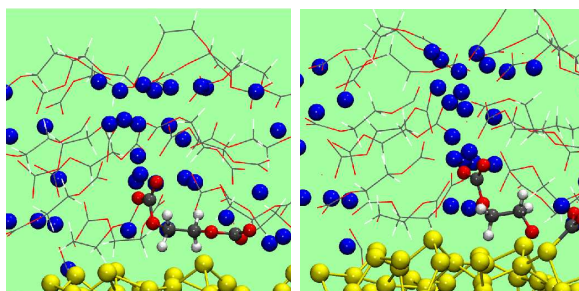


FIG. 4: NEB reaction energy profiles, illustrating reaction barriers and exothermicities. (a) LEDC on Li(100), red and blue denote the detachment of first a  $\text{CO}_2^{2-}$  and then a  $\text{O}^{2-}$ ; (b)  $\text{CO}_2^{2-}$  reaction on Li(100); (c) LEDC on a-Si, red and blue denote formation of C-Si bond and then breaking of C-O bond; (d)  $\text{Li}_2\text{CO}_3$  decomposition on Li(100); (e) a lower barrier  $\text{Li}_2\text{CO}_3$  reaction on Li(100) surface with 2 extra Li inserted at the interface, with  $\text{Li}_2\text{CO}_3$  bending and C-O bond-breaking depicted in red and blue, respectively; (f) out-of-plane bending of a single  $\text{Li}_2\text{CO}_3$  unit on Li(100), where red and green denote PBE and PBE0 predictions. In panels (c) and (d), the final barrier heights are obtained by quasi-Newton, non-NEB optimization of approximate barrier-top configurations generated from almost-converged NEB runs.



(a)

(b)

FIG. 5: (a) LEDC on a-Si surface. (b) C-O bond cleavage.

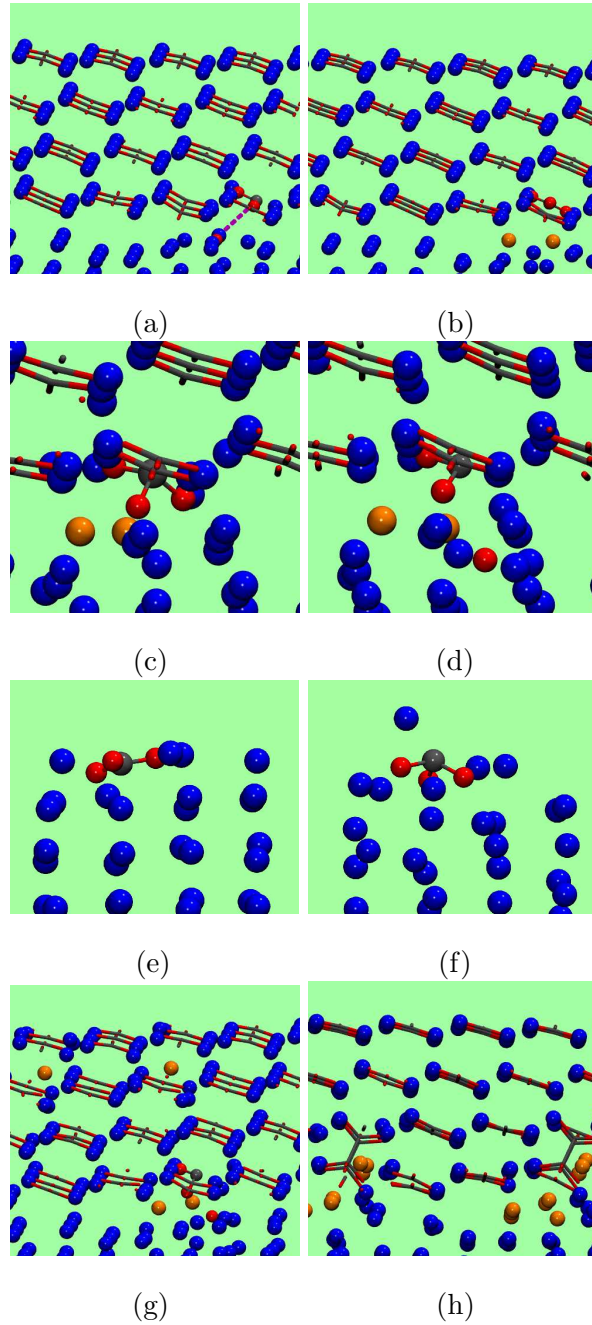


FIG. 6: (a)  $\text{Li}_2\text{CO}_3$  (001) on  $\text{Li}(100)$ , with broken C-O bond (red line) at interface; (b) intact  $\text{Li}_2\text{CO}_3$  but with 2 extra Li at interface; (c) reaction intermediate with C-atom out of plane; (d) final configuration with broken C-O bond. (e) A single  $\text{CO}_3^{2-}$  on  $\text{Li}(100)$ ; (f) bent geometry intermediate. (g) Same as panel (d), but with two  $\text{Li}^+$  interstitials between the top-most  $\text{LiCO}_3$  layers. (h) Spontaneous reactions forming 4 C-C bonds when 12 extra Li are added at interface, and 6 Li are inserted as interstitials between the  $\text{Li}_2\text{CO}_3$  layers closest to the Li surface. Extra Li are shown in orange.



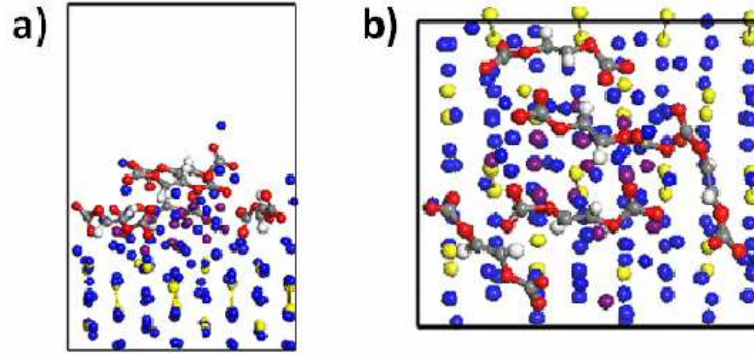


FIG. 7: (a)&(b) Side and top views of the five  $\text{Li}_2\text{VDC}$  oligomers adsorbed at the surface of the Li-covered lithiated Si anode. C, O, H, Li, and F atoms are represented by gray, red, white, blue, and purple spheres, respectively. The  $\text{LiPF}_6$  unit and FEC molecules are removed for clarity.

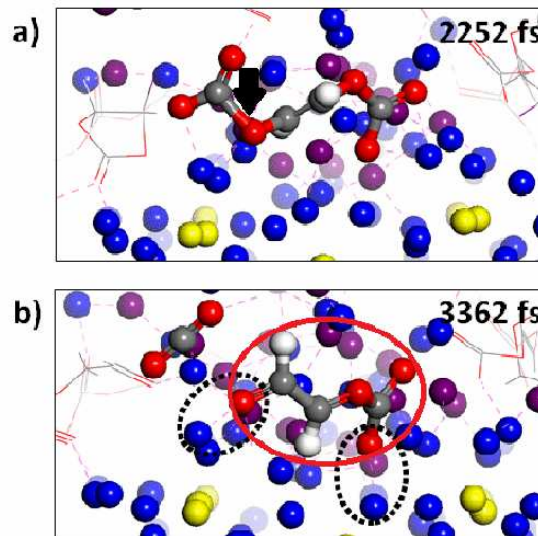


FIG. 8: Zoomed-in snapshots showing the time evolution of the LiF cluster covered  $\text{Li}_{13}\text{Si}_4$  (010) surface in contact with the 1.0 M  $\text{LiPF}_6/\text{FEC}$  electrolyte solution and 5  $\text{Li}_2\text{VDC}$  oligomers adsorbed on the surface (3 on the exposed area and 2 on top of the LiF cluster). (a) 2.252 ps; (b) 3.362 ps. Only the dissociating  $\text{Li}_2\text{VDC}$  oligomer is shown. FEC molecules are shown in a line display style. For clarity, a depth cue was applied to sharply focus on the dissociated oligomer and nearest atoms. Distant atoms and molecules appear blurrier.